# Controllable chip-based beam splitter for cold polar molecules

Xueyan Xu,[1,2] Tao Yang,[2] Shunyong Hou,[2,*] and Jianping Yin[2,†]
[1]*School of Electronic Engineering, Chaohu College, Heifei 238000, China*
[2]*State Key Laboratory of Precision Spectroscopy, East China Normal University, Shanghai, 200062, China*

(Received 24 March 2019; published 15 July 2019)

We proposed a Y-shaped molecular beam splitter for guided polar molecules, composed by several 1-$\mu$m-thick gold electrodes deposited on a chip. The splitter has a total length of 10 mm and the height of the electrostatic guiding center (minimum of the electric fields) is about 100 $\mu$m from the surface of the chip. Our theoretical analysis and trajectory calculations are carried out using two types of polar molecules of ammonia-$D_3$ ($ND_3$) and strontium fluoride (SrF). The calculated results show explicitly that, by applying a few hundred volts on the electrodes, the splitter can direct the guided (light or heavy) polar molecules to either of the two outgoing arms with any desired ratio (from 0% to 100%) by changing the voltages applied on the electrodes. This chip-scale molecular beam splitter offers a platform for molecular optics, precision measurements, and quantum computation. This basic optical element could be integrated into molecular chips and serve as a building block for a future gas-phase molecular laboratory on a chip.

DOI: 10.1103/PhysRevA.100.013411

## I. INTRODUCTION

Lab-on-a-chip technology is now increasingly pursued by both physicists and chemists, because it allows precise control of particles, enjoys fast transport times and accurate knowledge of molecular concentrations, and permits setup miniaturization, as well as low cost and power [1]. Significant advances have been made in atomic chips [2] for their excellent applications, such as fast Bose-Einstein condensate (BEC) generation [3], and precision measurements [4]. Although the molecular chip is still in its infant stage compared to the atomic chip, considerable progress in the molecular chip has been made in recent years. Various chip-based molecular optical elements have been demonstrated or proposed, such as the Stark decelerator [5,6], molecular mirror [7,8], trap [9], and electrostatic lattice [10]. Most recently, an improved chip-based molecular clock has been demonstrated and shows more advantages over chip-scale atomic clocks [11]. Of them the molecular beam splitter is an essential optical element required in the fields of molecular optics and molecular interferometry. The first chip-based atomic beam splitter was demonstrated almost two decades ago [12,13]. However, little work has been done on a chip-scale molecular beam splitter.

Recently, many macroscopic molecular beam splitters have been well demonstrated. In 2011, our group experimentally demonstrated an electrostatic molecular beam splitter for polar molecules [14], which consists of a Y-shaped charged wire and a metallic plate capacitor. In 2017, Palmer and Hogan demonstrated a Rydberg-atom beam splitter [15], composed of a metallic plate and two-dimensional electrodes. In the same year, Gordon and Osterwalder experimentally demonstrated a three-dimensional (3D)-printed macroscopic beam splitter for polar neutral molecules [16]. These excellent works have paved the way for studies of cold molecular physics and molecular optics. However, limited by their complex structures, it is difficult to miniaturize these devices and integrate them onto the chip surface. Here we present a chip-scale beam splitter scheme for cold polar molecules, which has a concise and robust structure. By applying a few hundred volts on the electrodes, a Y-shaped guiding tube for low-field-seeking state polar molecules can be formed in the vicinity of the chip, allowing dividing one guided (light or heavy) molecular beam into two parts with any desired ratio. In the following sections we will give a detailed introduction to the design and operation principle of the chip-based molecular beam splitter. Following that, Monte Carlo simulations and theoretical analyses using two types of polar molecules, $ND_3$ and SrF, will be carried out to show the performance of the beam splitter. Finally, there is Discussion and Conclusions section.

## II. SCHEME AND OPERATION PRINCIPLE

The schematic of our chip-based molecular beam splitter is modeled in Fig. 1. It consists of several 1-$\mu$m-thick gold electrodes, which are deposited onto a glass substrate and patterned like a Y. The geometry dimension of the scheme is labeled in Fig. 1. In the following tests the parameters are set as follows: The length of the front (straight) part and the back (branch) part is $c = 5$ mm and $d = 5$ mm, respectively. Thus the total length of the beam splitter is 10 mm. The width of the straight electrodes is $a = 120\,\mu$m and the gap between them is $g = 100\,\mu$m. The middle straight electrode is equally divided into two parts with a gap of $g_0 = 10\,\mu$m. The width of the branch electrodes is $b = 100\,\mu$m and the gap between them is also 100 $\mu$m. The diverging angle is $2\theta = 10.28^\circ$. The potential applied on each electrode is labeled in Fig. 1 and is given by

$$U_i = (-1)^{i+1} U_0[1 + \cos(i4\pi/3 + \phi)] \quad (\text{for } i = 1, 2, 3), \tag{1}$$

*syhou@lps.ecnu.edu.cn
†jpyin@phy.ecnu.edu.cn

 

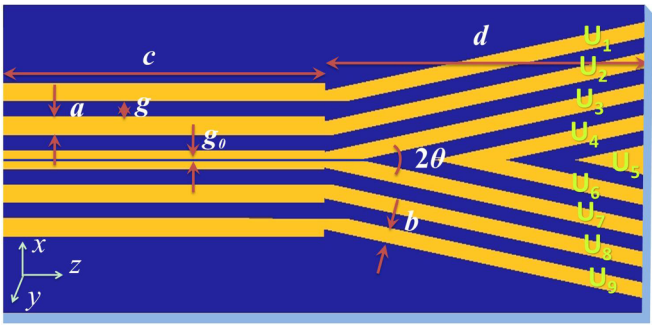


FIG. 1. Schematic diagram of the molecular beam splitter, together with the geometric parameters of the electrodes and the applied voltage on each electrode. A definition of the coordinate system used in the text is also given, where molecules propagate along the $z$ axis.

and $U_7 = -U_3$, $U_8 = -U_1$, $U_9 = -U_2$, $U_4 = U_6 = -U_0$, $U_5 = U_0$, where $i$ is the index of the electrodes. Here $\phi$ is an important parameter used to change the potential on each electrode and thus to adjust the beam splitting ratio. The splitting ratio is defined as the ratio of the molecular number of each branch to the total number of the two branches. It should be noted that as the parameter $\phi$ gets larger than 180°, the potential is applied as follows:

$$U_i = (-1)^{i+1} U_0 \{1 + \cos[(10 - i)4\pi/3 + \phi]\} \quad (\text{for } i = 7, 8, 9), \tag{2}$$

and $U_7 = -U_3$, $U_8 = -U_1$, $U_9 = -U_2$, $U_4 = U_6 = -U_0$, $U_5 = U_0$. With these settings, this very simple and robust structure can produce a two-dimensional Y-shaped hollow guiding tube for the low-field-seeking state polar molecules above the surface of the electrodes.

The splitting ability of the beam splitter strongly depends on both the depth of the guiding potential and the splitting angle of the two output arms. In principle, larger applied voltages and smaller diverging angles are able to tame the molecules of higher velocities. If the value of the molecular beam velocity is so high that it is beyond the splitting ability of the splitter, the molecules will pass through the guiding potential and fail being split. In the following calculations and simulations the potential $U_0$ is set to 500 V. With the help of finite-element methods, the electric field distribution of the beam splitter above the chip is calculated. Figure 2(a) shows the contours of the electric field magnitude in the $xy$ plane at four selected positions: A ($z = 4.0$ mm), B ($z = 6.0$ mm), C ($z = 7.0$ mm), and D ($z = 8.0$ mm), with the setting of $\phi = 180°$. It is clear that the two outgoing arms are gradually formed along the $z$ axis. The height of the electrostatic guiding center (minimum of the electric fields) is about 100 $\mu$m from the chip. It is worth noting that the splitting point of the potentials is at $z = 6.6$ mm, a little bit different from the geometrical splitting point of the splitter (i.e., $z = 5.0$ mm). We take $ND_3$ as a tester. The force experienced by a $ND_3$ molecule is derived from the Stark potential utilizing the formula

$$F(r) = -\nabla W_s(r) = -\left(\frac{dW_s}{dE}\right)\nabla|E(r)|, \tag{3}$$

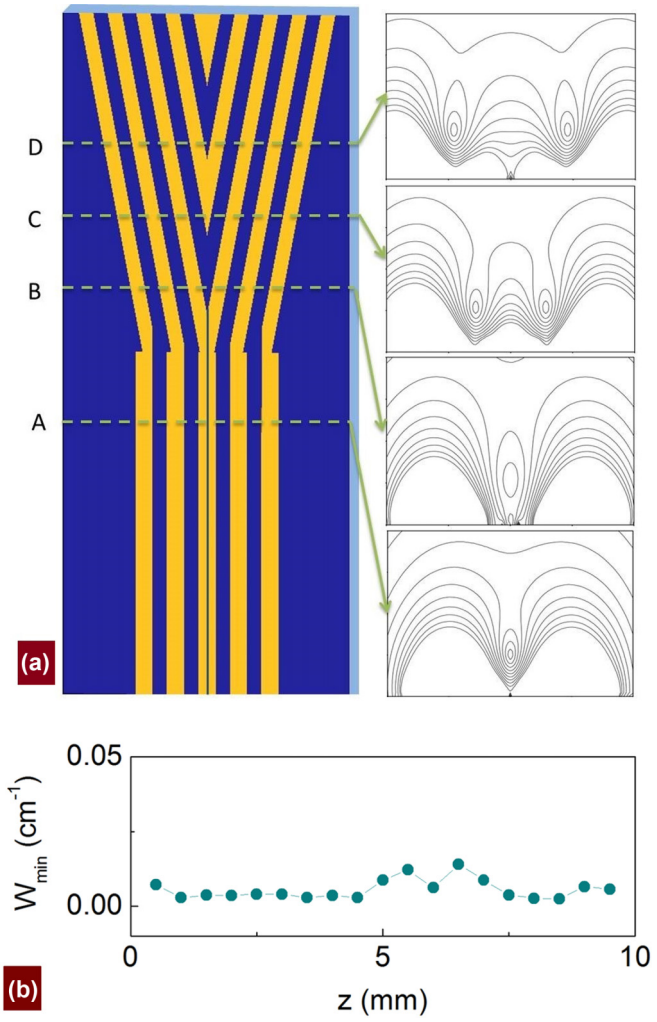


FIG. 2. (a) Electric field distribution of the beam splitter for $\phi = 180°$ in four typical planes perpendicular to the $z$ axis (A: $z = 4.0$ mm, B: $z = 6.0$ mm, C: $z = 7.0$ mm, D: $z = 8.0$ mm). The contour lines are displayed in intervals of 2.0 kV/cm. (b) The local minimum of the splitting guiding potential tube(s) along the $z$ direction.

where $W_s$ is the Stark potential energy and $\boldsymbol{E}$ is the electric field strength. The direction of force points towards higher fields for levels with $KM > 0$ (high-field-seeking states), and towards lower fields for levels with $KM < 0$ (low-field-seeking states). In electric fields below 100 kV/cm, the interaction between the different rotational levels can be neglected for $ND_3$ molecules, and the Stark energy can be well approximated as follows:

$$W_s = \pm\sqrt{\left(\frac{W_{\text{inv}}}{2}\right)^2 + \left(\mu_0|E|\frac{MK}{J(J+1)}\right)^2} - \frac{W_{\text{inv}}}{2}, \tag{4}$$

where $W_{\text{inv}}$ is the zero-field inversion splitting (0.053 $\text{cm}^{-1}$ for $ND_3$ [17]), and $M$, $K$ are the projection of the total angular momentum $\boldsymbol{J}$ on the electric field $\boldsymbol{E}$ and on the symmetry axis, respectively. $\mu_0$ is the permanent electric dipole moment (1.5 D for $ND_3$ [18]). For $ND_3$ in the $|J, KM\rangle = |1, -1\rangle$ state the transverse motion near the center of the guiding tube is harmonic. The expression of the potential well can be given

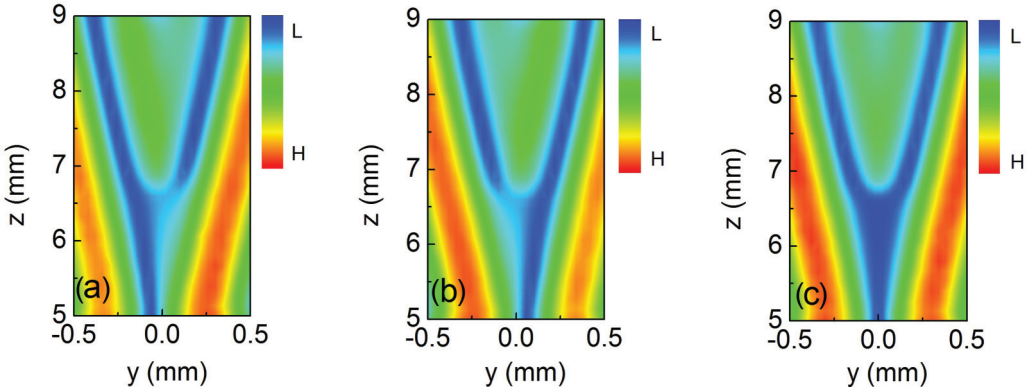


FIG. 3. Electric field distribution in the plane parallel to the chip at the height of 100 $\mu$m for $\phi = 140^\circ$ (a), $\phi = 220^\circ$ (b), and $\phi = 180^\circ$ (c), respectively. Color bar labels H and L mean high and low electric field, respectively.

by $U_y = k_y y^2/2$, where $k_y = m\omega_y^2$. This yields a transverse trap frequency $f_y = \omega_y/2\pi = 36$ kHz in the straight guiding arm, and a depth of 120 mK. The two output arms have nearly the same characteristics as the input guiding tube, except that the depth and transverse trap frequency are both a little bit lower than the input guiding tube, that is, 100 mK and 33 kHz, respectively.

As can be seen from Fig. 2(b), two potential hills ($\sim 0.011\,\mathrm{cm}^{-1}$) emerge near the splitting point, which can stop $ND_3$ molecules with velocities below 3.5 m/s (0.5 m/s for the SrF molecule). Such a tiny roughness therefore has almost no effect on normal splitting experiments, but it is unfavorable for the interferometric applications. These barriers can be minimized through parameter optimization or structure modification. Additionally, in the interferometric experiments the molecular beams normally move very slowly such that the applied voltages on the splitter would be reduced and thus this roughness will decrease correspondingly. As mentioned before, the guiding tube of the output arms can be adjusted by changing the value of $\phi$. Figure 3 depicts the electric field distribution in the plane parallel to the chip at the height of 100 $\mu$m for three different values of $\phi$. It explicitly shows the paths diverge in the region. As can been seen from Figs. 3(a) and 3(b), the right (left) output arm is almost closed near the splitting point for $\phi = 140^\circ$ ($\phi = 220^\circ$); thus most molecules are directed to the left (right) output arm. Figure 3(c) shows the case for $\phi = 180^\circ$, where the electric field distribution of the two branches is spatially symmetric relative to the incoming guide axis ($z$ axis). As a result, the guided molecules split evenly into two sides and the splitting ratio of the two arms will be equal. Therefore, it is possible to control the ratio between the two arms by changing the value of $\phi$, i.e., adjusting the applied voltages on the electrodes.

## III. MONTE CARLO SIMULATION AND ANALYSIS

In order to verify the performance of our proposal, $ND_3$ in the $|J, KM\rangle = |1, -1\rangle$ state is used to carry out 3D Monte Carlo simulations. Background collision and surface-induced heating losses are ignored in our simulation because present vacuum technology and cooling technology permit greatly reducing these losses [19]. Nonadiabatic transition loss is also not considered. The position and velocity distributions of the initial molecular beam are Gaussian in all directions with the six-dimensional (6D) emittance $[\Delta z \times \Delta v_z] \times [\Delta x \times \Delta v_x] \times [\Delta y \times \Delta v_y] = [1.0\,\mathrm{mm} \times 12.0\,\mathrm{m/s}] \times [0.5\,\mathrm{mm} \times 12.0\,\mathrm{m/s}] \times [0.5\,\mathrm{mm} \times 12.0\,\mathrm{m/s}]$. The beam contains 500 000 molecules with the initial distribution of the beam centered at $y = 0\,\mu$m, $v_y = 0$ m/s, $x = 100\,\mu$m, $v_x = 0$ m/s, $z = 0\,\mu$m, $v_z = 50$ m/s. The above parameters of the molecular beam are chosen by referring to some recent experimental results [6,20,21]. The molecular beam is first straightly guided for a distance of about 5 mm and then gradually split into two beams by the two branch arms after the splitting point.

The simulation results are shown in Fig. 4. The profiles of the molecular number density are plotted as a function of the transverse position for four selected values of $\phi$. The profiles are obtained by measuring the guided $ND_3$ molecules at the two outlets of the beam splitter. When $\phi = 180^\circ$, $U_1 = U_9 = 750$ V, $U_2 = U_8 = -750$ V, $U_3 = U_7 = 0$ V, $U_4 = U_6 = -500$ V, $U_5 = 500$ V, the voltages on the electrodes are symmetric relative to the $z$ axis. Due to its inherent symmetry of the guiding electric fields, the $ND_3$ molecular beam is divided into two equal parts, as shown in Fig. 4. The transverse temperature of the straightly guided molecular beam is 40 mK, whereas the transverse temperature of the beams in the branch arms is slightly lower, that is,

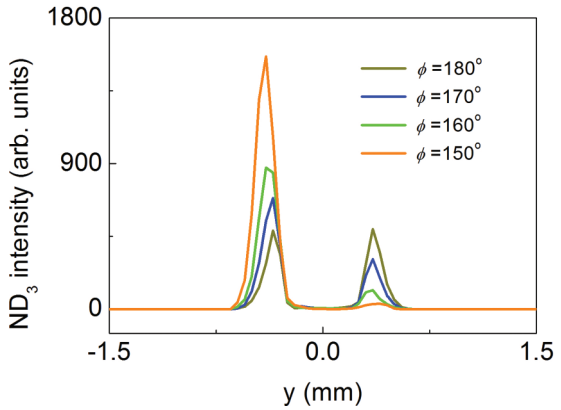


FIG. 4. Simulated transverse profiles of the guided $ND_3$ molecules measured at the two outlets of the molecular splitter for four selected values of $\phi$.

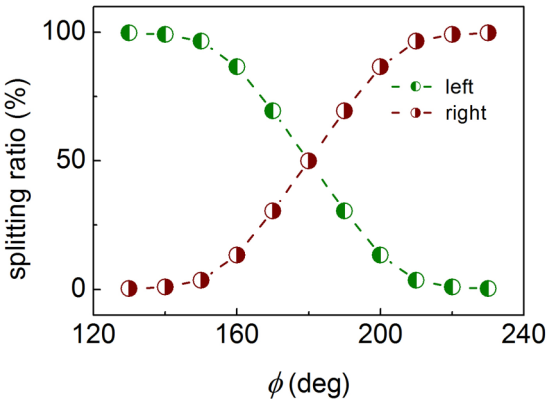


FIG. 5. Dependences of the splitting ratio of the molecular beam splitter on the value of $\phi$ (simulated results).

38 mK. The transverse temperature is obtained using the following expressions: $(2/2)k_B T_{\text{trans}} = (1/2)k_B T_x + (1/2)k_B T_y$, and $T_{x,y} = m\Delta v_{x,y}^2/(8 \ln 2 k_B)$ [22]. When the value of $\phi$ decreases, the right guiding tube gradually begins to close, resulting in the left arm guiding more and more molecules than the right side, as shown in Fig. 4. The splitting ratio of the molecular beam splitter is plotted as a function of $\phi$ in Fig. 5. It is clear that the splitting ratio on the left is gradually increased along with lowering the value of $\phi$. When $\phi = 140^\circ$, a splitting ratio of $R = 0.9\% - 99.1\%$ is obtained. As the value of $\phi$ decreases to 130°, the guided molecular beam is absolutely directed to the left; i.e., a splitting ratio of $R = 0\% - 100\%$ is obtained. Similarly, more and more molecules are directed to the right along with raising the value of $\phi$, and finally all molecules turn right when $\phi = 230^\circ$. We know from these simulations that it is possible to divide one molecular beam into two beams of any proportion using our chip-based electrostatic molecular beam splitter.

Generally, interference experiments with massive particles are considered to be the ultimate demonstration of the quantum nature of these objects [23]. Therefore it would be interesting and worthwhile to design a beam splitter for heavy molecules. However, it is usually more difficult to manipulate heavy polar molecules (roughly defined as >100 amu) because their Stark curve of the rotational energy levels easily turns down in high electric fields, as well as their more kinetic energy for a given velocity. The two-dimensional guiding tubes originated from our beam splitter electrodes can offer deep potential wells and thus allow taming both light and heavy polar molecules. The $^{88}$SrF molecule is a typical heavy polar molecule that is amenable to laser cooling [24]; therefore we selected SrF in the $|N, N_M\rangle = |2, 0\rangle$ state as a tester to verify our chip-based beam splitter. Here $N$ is the rotational number and $N_M$ is the projection of $N$ on the electric field axis. Since the maximum transverse electric field is around 35 kV/cm, the SrF molecule in the $|N, N_M\rangle = |2, 0\rangle$ state is always low-field seeking in the guiding tubes. Stark shift of SrF of the lowest rotational levels in the vibronic ground state can be found elsewhere [25]. The force experienced by the SrF molecule in the electrostatic fields can be deduced from the formula (3). For the SrF molecule, the beam splitter parameters are $2\theta = 6.0^\circ$, $c = 3.0$ mm, $d = 7.0$ mm. All other parameters of the splitter are identical to the above ones for $ND_3$ molecule. The molecular beam parameters are $[\Delta z \times \Delta v_z] \times [\Delta x \times \Delta v_x] \times [\Delta y \times \Delta v_y] = [0.5\,\text{mm} \times 5.0\,\text{m/s}] \times [0.5\,\text{mm} \times 5.0\,\text{m/s}] \times [0.5\,\text{mm} \times 5.0\,\text{m/s}]$, and the total molecular number is also 500 000. Our simulated results show that, similar to the case of $ND_3$, by changing the value of $\phi$, SrF molecules can turn either left ($\phi < 180^\circ$) or right ($\phi > 180^\circ$) with any desired ratio. When $\phi = 180^\circ$, the SrF molecular beam is equally divided into two parts (not shown). Splitting ratios $R = 1.5\% - 98.5\%$, and $R = 0\% - 100\%$ are obtained for $\phi = 130^\circ$ and $\phi = 120^\circ$, respectively (not shown). When $\phi = 240^\circ$, all SrF molecules are directed to the right. It shows that heavy polar molecules are also amenable to our designed chip-based molecular beam splitter, which offers more possibilities for basic research and application work.

## IV. DISCUSSION AND CONCLUSIONS

In summary, we have presented a centimeter-size molecular beam splitter, realized with simple wires on chip surfaces, which is capable of splitting beams of cold (light or heavy) molecules into spatially separated components in the vicinity of a chip. It is very easy to adjust the splitting ratios of the two outgoing arms (from 0% to 100%) by changing the voltages applied on the electrodes. Note that we choose the geometries of the electrodes for the convenience of discussion, which are subject to scaling on a practical basis.

Such a robust and easy to operate molecular beam splitter may find some important applications in the fields of integrated molecule optics, cold molecular collision, precise measurement, and even quantum computation. For instance, in some molecular collision experiments [26], while one of the split components of a molecular beam is being used as an intensity reference, the other split beam component collides with the target atoms (or molecules). If guiding a coherent ultracold molecular beam such as molecular Bose-Einstein condensate, the device could act as a coherent molecular beam splitter and can be used for molecular interference experiments. Since the beam splitter allows directing the guided beam to either of the outgoing arms, it can serve as an electric switch for integrated molecular optics. In 2001 Knill *et al.* presented a protocol of creating a universal quantum computer solely with a beam splitter (and other auxiliary components) [27], where the beam splitter is used for operating photons. By extension, it might be possible to create a counterpart quantum computer using a miniature molecular beam splitter, if using polar molecules as qubits [28–32]. In a word, this basic optical unit could be integrated into molecular chips and contribute to future lab-on-a-chip technology. Our experimental setup is currently under construction.

## ACKNOWLEDGMENTS

This work is supported by the National Natural Science Foundation of China (Grants No. 11834003, No. 91536218, No. 11034002, No. 11274114, No. 11504112, and No. 11874151); the National Key Basic Research and Development Program of China (Grant No. 2011CB921602); the Key

Program of Natural Science Research of Higher Education Universities of Anhui Province (Grant No. KJ2019A0684); the Key Foundation for Outstanding Young Scientists of Higher Education Institutions in Anhui Province, China (Grant No. gxyqZD2016286); and the Fundamental Research Funds for the Central Universities, Shanghai Pujiang Talents Plan (18PJ1403100), Exploration Funds for the Shanghai Natural Science Foundation (18ZR1412700).

[1] G. Santambrogio, EPJ Tech. Instrum. **2**, 14 (2015).
[2] M. Keil, O. Amit, S. Zhou, D. Groswasser, Y. Japha, and R. Folman, J. Mod. Opt. **63**, 1840 (2016).
[3] W. Hänsel, P. Hommelhoff, T. W. Hänsch, and J. Reichel, Nature **413**, 498 (2001).
[4] S. Abend, M. Gebbe, M. Gersemann, H. Ahlers, H. Müntinga, E. Giese, N. Gaaloul, C. Schubert, C. Lämmerzahl, W. Ertmer, W. P. Schleich, and E. M. Rasel, Phys. Rev. Lett. **117**, 203003 (2016).
[5] S. A. Meek, H. L. Bethlem, H. Conrad, and G. Meijer, Phys. Rev. Lett. **100**, 153003 (2008).
[6] S. A. Meek, H. Conrad, and G. Meijer, Science **324**, 1699 (2009).
[7] S. A. Schulz, H. L. Bethlem, J. van Veldhoven, J. Küpper, H. Conrad, and G. Meijer, Phys. Rev. Lett. **93**, 020406 (2004).
[8] A. I. G. Flórez, S. A. Meek, H. Haak, H. Conrad, G. Santambrogio, and G. Meijer, Phys. Chem. Chem. Phys. **13**, 18830 (2011).
[9] B. G. U. Englert, M. Mielenz, C. Sommer, J. Bayerl, M. Motsch, P. W. H. Pinkse, G. Rempe, and M. Zeppenfeld, Phys. Rev. Lett. **107**, 263003 (2011).
[10] S. Hou, B. Wei, L. Deng, and J. Yin, Phys. Rev. A **96**, 063416 (2017).
[11] C. Wang, X. Yi, J. Mawdsley, M. Kim, Z. Wang, and R. Han, Nat. Electron. **1**, 421 (2018).
[12] D. Cassettari, B. Hessmo, R. Folman, T. Maier, and J. Schmiedmayer, Phys. Rev. Lett. **85**, 5483 (2000).
[13] D. Müller, E. A. Cornell, M. Prevedelli, P. D. D. Schwindt, A. Zozulya, and D. Z. Anderson, Opt. Lett. **25**, 1382 (2000).
[14] L. Deng, Y. Liang, Z. Gu, S. Hou, S. Li, Y. Xia, and J. Yin, Phys. Rev. Lett. **106**, 140401 (2011).
[15] J. Palmer and S. D. Hogan, Phys. Rev. A **95**, 053413 (2017).
[16] S. D. S. Gordon and A. Osterwalder, Phys. Rev. Appl. **7**, 044022 (2017).
[17] L. Fusina and G. D. Lonardo, J. Mol. Spectrosc. **112**, 211 (1985).
[18] G. Dilonardo and A. Trombetti, Chem. Phys. Lett. **84**, 327 (1981).
[19] S. A. Meek, G. Santambrogio, B. G. Sartakov, H. Conrad, and G. Meijer, Phys. Rev. A **83**, 033413 (2011).
[20] F. M. H. Crompvoets, R. T. Jongma, H. L. Bethlem, A. J. A. van Roij, and G. Meijer, Phys. Rev. Lett. **89**, 093004 (2002).
[21] S. Hou, S. Li, L. Deng, and J. Yin, J. Phys. B: At., Mol. Opt. Phys. **46**, 045301 (2013).
[22] M. Gupta and D. Herschbach, J. Phys. Chem. A **103**, 10670 (1999).
[23] T. Juffmann, A. Milic, M. Müllneritsch, P. Asenbaum, A. Tsukernik, Jens Tüxen, M. Mayor, O. Cheshnovsky, and M. Arndt, Nat. Nanotechnol. **7**, 297 (2012).
[24] E. S. Shuman, J. F. Barry, and D. DeMille, Nature **467**, 820 (2010).
[25] S. Hou, B. Wei, L. Deng, and J. Yin, Sci. Rep. **6**, 32663 (2016).
[26] V. Zhelyazkova and S. D. Hogan, Phys. Rev. A **95**, 042710 (2017).
[27] E. Knill, R. Laflamme, and G. J. Milburn, Nature **409**, 46 (2001).
[28] D. DeMille, Phys. Rev. Lett. **88**, 067901 (2002).
[29] S. F. Yelin, K. Kirby, and R. Côté, Phys. Rev. A **74**, 050301(R) (2006).
[30] A. André, D. Demille, J. M. Doyle, M. D. Lukin, S. E. Maxwell, P. Rabl, R. J. Schoelkopf, and P. Zoller, Nat. Phys. **2**, 636 (2006).
[31] E. Kuznetsova, R. Côté, K. Kirby, and S. F. Yelin, Phys. Rev. A **78**, 012313 (2008).
[32] P. Rabl, D. DeMille, J. M. Doyle, M. D. Lukin, R. J. Schoelkopf, and P. Zoller, Phys. Rev. Lett. **97**, 033003 (2006).